

A Comprehensive Convolutional Neural Network Architecture Design using Magnetic Skyrmion and Domain Wall

Saumya Gupta¹, Venkatesh Vadde¹, Bhaskaran Muralidharan¹, and Abhishek Sharma²^{*}
¹*Department of Electrical Engineering, Indian Institute of Technology Bombay, Powai, Mumbai-400076, India and*
²*Department of Electrical Engineering, Indian Institute of Technology Ropar, Rupnagar, Punjab-140001, India*

(Dated: July 12, 2024)

Spintronic-based neuromorphic hardware enables high-density and rapid data processing at nanoscale lengths. Leveraged by the topologically protected spin configurations and low current densities to manipulate magnetic structures such as skyrmion and domain wall. The paper presents a compact, energy-efficient multi-bit skyrmionic synapse and domain wall-based ReLU with max-pooling functionalities for hardware neural network applications. A 4-bit, 5-bit, and 6-bit skyrmionic synapse is proposed, featuring a circular bilayer vortex-based geometry. The 4-bit skyrmionic synapse consumes an ultra-low energy of 0.8724 fJ per weight update. The proposed skyrmionic synapse comprises an ultra-thin ferromagnetic layer with a strong Dzyaloshinskii-Moriya interaction and a polarizer layer with a vortex-like spin configuration. The interaction between perpendicular current flow and the labyrinth maze-like uniaxial anisotropy profiles induce skyrmionic gyration, resulting in long-term potentiation (LTP) and long-term depression (LTD) that modifies the synaptic weights. We develop a phenomenology of the synaptic device, implementing 16-state (4-bit), 32-state (5-bit), and 64-state (6-bit) skyrmionic synapses, analyzing them quantitatively using micromagnetics simulations. Furthermore, we design a CMOS hybrid domain wall-based ReLU-max pooled circuit. The activation function works on the variation of the domain wall position implying variation in the device resistance on encountering uniaxial anisotropy variation along the track. To demonstrate the practical application of our 4-bit (16-state) skyrmionic synapse with domain wall-based ReLU-Max Pooling circuit we integrate it into an inference-based convolutional neural network (CNN) for pattern recognition, achieving a comparable accuracy of 98.07% to software-based ideal training.

I. INTRODUCTION

Artificial intelligence[1] simulates human cognition, demanding substantial resources to handle the exponential data growth. In contrast, neuromorphic computing[2] emulates the human brain structure and functionality adapting to more complex tasks, achieving lower power consumption. The ability to train an artificial neural network (ANN) model with minimal power consumption is one of the key features of neuromorphic computing over Von-Neumann architecture. While, the conventional Moore approach, relies on CMOS technology, exploring beyond Moore by investigating spintronics-based neuromorphic[3] circuitry presents a promising alternative for low-power devices and systems. Various emerging spintronics-based neuromorphic devices include LIF-based neurons[4, 5], skyrmion-based synapses[6], adaptive neurons[7], and domain wall-based adders[8]. Magnetic skyrmions, two-dimensional solitons with local spin whirls in magnetic materials [9], have attracted significant interest for in-memory[10] computation. They have been extensively studied in ultra-thin ferromagnetic films and non-centrosymmetric magnetic bulk crystals, considering interfacial and bulk Dzyaloshinskii-Moriya interactions [11].

Skyrmions offer advantages such as small size, topological stability, ultra-low power depinning current den-

sity, along with particle-like characteristics[12] having the ability to accumulate within a compact area without interacting with topological defects, making them suitable for synaptic devices in neuromorphic computing. The spin-orbit torque driven domain walls are widely explored for synapse, memory and logic operations[13–15]. The non-volatility offered by the domain wall's position makes it useful for in-memory computation. The persistent domain wall velocity even after the current is turned off hinders the realization of a practical synapse device. Additional design specifications such as pinning(with notches or grooves)[16] is required for controlled retention and stability in the domain wall based device making it susceptible to creep[17, 18] issues.

Most spintronic-based hardware neural networks feature a segment of the network as their key spintronics component, complemented by a software-based activation and pooling functions[15][6][19][20][21][22], which makes it difficult to gauge the full potential of the maximal spintronic network. We approach maximal spintronic convolutional neural network implementation using magnetic skyrmion(convolution) and domain wall(Activation and pooling functionalities simultaneously). Traditionally in a spintronic based synapse[23], accommodating more states requires increased device length, which raise concerns about the shape anisotropy and multiple domain formation. Skyrmions, benefiting from topological protection, are more robust than domain walls as they can accommodate in circular geometries allowing for smaller device size compared to domain wall-based synapses. Skyrmions stable configu-

* abhishek@iitrpr.ac.in

ration renders them immune to the persistent velocity issue observed in domain walls. Hence, we have preferred Skyrmions over domain walls for synapse operation due to their scalability, which translates into more states. However, we preferred domain walls more in the case of the activation function due to a faster reset (few ns) of the activation function with variable input compared to skyrmion (reset in ≈ 500 ns)[24].

To address the demand for maximal hardware implementation for an energy-efficient neural network, we propose a strategic placement and design of a skyrmion-based synapse and a CMOS hybrid Domain wall-based ReLU-Max Pooling circuit to implement the CNN architecture.

Skyrmion-based synapse is implemented with a labyrinth maze-like (unicursal: one path that leads you from the entrance to the center) uniaxial anisotropy profiles for 4-bit and 5-bit synapse designs. Furthermore, we have shown the scalability of our compact synapse device up to 6-bit, tackling issues related to shape anisotropy. The topologically protected, compactly packed skyrmions are highly advantageous compared to other reported long-range devices[23] for synapse operation, as they offer more conductance states in a compact space subjecting to a linear and symmetric weight update. The domain wall-based ReLU is a hybrid spintronic-CMOS device that utilizes a uniaxial anisotropy variation to modify the resistance value linearly following the domain wall positions. Thus, obtaining the activation and max-pooling functionalities simultaneously for application in the CNN network. Unlike MTJ-based ReLU circuits, which require significantly higher current densities[25] and thus undermine energy efficiency, our device represents a major improvement by maintaining low current requirements and achieving the same functionality.

We demonstrate a full hardware functionality of skyrmion-based synapse and CMOS hybrid domain wall-based ReLU-Max Pooling in a CNN for pattern recognition using the MNIST handwritten & fashion MNIST data set and low power consumption elements for neuromorphic computing hardware. Simulations show the skyrmion and domain wall-based CNN achieves an accuracy of approximately 98.07%, comparable to software-based training accuracy of around 98.35%

The rest of the paper is organized as follows. In Sec.II, we describe our proposed Skyrmionic synapse, domain wall-based ReLU, and Max Pooling design. Sec.III describes the mathematical and simulation framework of our devices. In Sec. IV, we discuss the results obtained from the simulation, followed by V describing the CNN implementation of our device, and finally, Sec. VI concludes the paper.

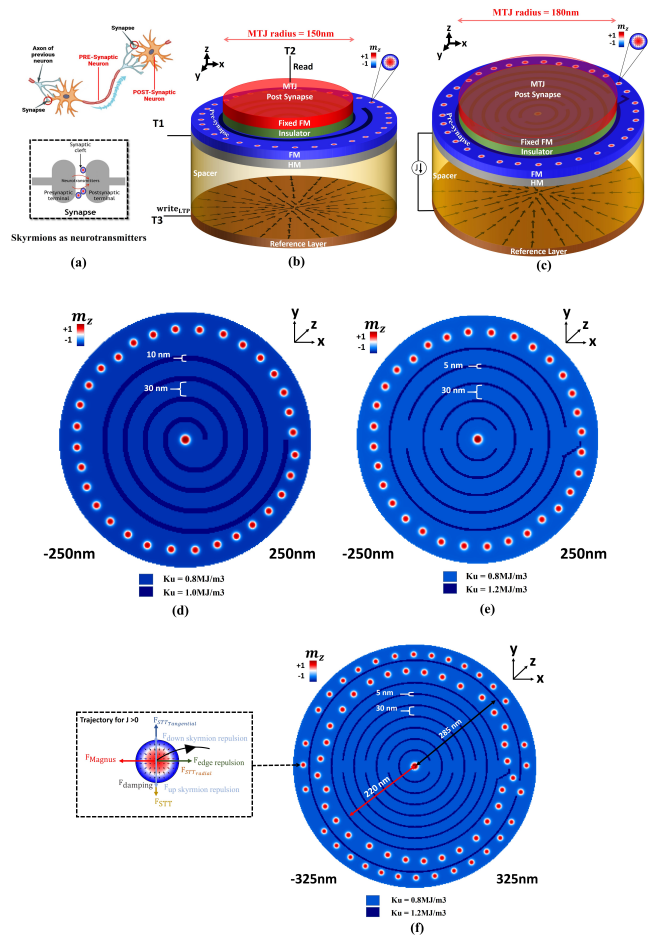


FIG. 1. (a) Schematic of a biological neuron connected via a synapse. The black box: Analogy between the biological neural network and our proposed synapse device. A 3D schematic of the proposed magnetic skyrmion-based 5-bit artificial Synapse (b) with spiral Uniaxial anisotropy profile. (c) with concentric Uniaxial anisotropy profile. The top view schematic of a skyrmionic synapse device shows 32 skyrmions around the periphery and one skyrmion pinned at the center (d) with spiral-like uniform uniaxial anisotropy (e) with a concentric-like uniform uniaxial anisotropy profile & an L shaped wedge extension. (f) The top view schematic of a 6-bit skyrmionic synapse device shows 64 skyrmions around the periphery in a concentric compact design with one skyrmion pinned at the center having a concentric-like uniform uniaxial anisotropy profile & a L shaped wedge extension. The dotted black box depicts forces on the skyrmion. The magnetization direction is color-coded: blue is into the plane, white is in the plane, and red is out of the plane.

II. DEVICE MODEL

A. Background

We present the design of two major spintronics-based counterparts for the synapse and ReLU function to implement a hardware convolutional network.

The biological neural network comprises neurons interconnected through synapses, as depicted in Fig.1a synapse typically consists of three components: a pre-synaptic region, a synaptic cleft, and a postsynaptic region.

In our case, skyrmions function as neurotransmitters, being stored and released by the pre-synaptic region, while the postsynaptic region receives them. During synaptic transmission, an electrical pulse triggers the skyrmions to move individually from the pre-synaptic region to the postsynaptic region, facilitated by the synaptic cleft: a narrow gap between the pre-and postsynaptic regions. Applying a positive current pulse causes skyrmions to travel from the pre-synaptic region to the postsynaptic region through the synaptic cleft, leading to LTP. Conversely, a negative current pulse induces skyrmions to move from the postsynaptic region back to the pre-synaptic region via the synaptic cleft, resulting in LTD.

The CNN implementation also requires an activation and max-pooling function. While the activation function facilitates complex data learning by introducing non-linearity in the system, the max-pooling function selects the maximum element of the feature map, pooling all the important features from the image.

In the paper, the activation function(ReLU) is implemented using a SOT-based domain wall device integrated with an MTJ. The domain wall positions in the ferromagnet introduce non-linearity by returning zero for the domain wall positions that are not under the MTJ and allow values to pass through for the positions under the MTJ. The ReLU function rectifies the vanishing gradient descent problem in deep learning models providing an advantage over other activation functions such as Sigmoid and hyperbolic tangent function.

The 9-Input ReLU max-pooled network is a hybrid CMOS spintronic implementation of the max-pooling function for a maximal neuromorphic network hardware.

B. Skyrmionic synapse device

The proposed skyrmionic synapse device comprises two circular FM layers separated by an insulator, namely the Ferromagnet layer(FM) and the reference layer(RL). The FM layer is in contact with a heavy metal (HM) layer at the bottom, giving rise to the emergence of Dzyaloshinskii-Moriya interaction at the HM/FM interface. The FM layer has a perpendicular magnetic anisotropy(PMA), while the reference layer's magnetization is fixed, having a vortex-like spin polarization as shown in Fig.1(b). Also, Fig.1(b,c) depicts the complete device, showcasing the pre-synapse and post-synapse regions, analogous to the biological model as shown in Fig.1(a).

we simulated four skyrmionic synapse devices with

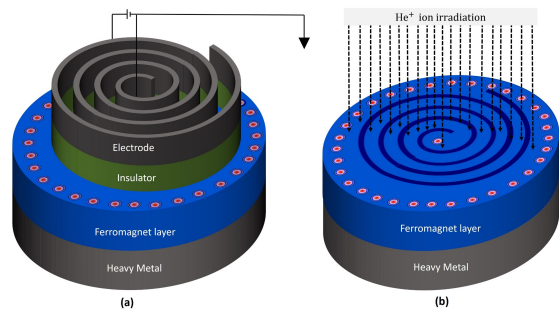


FIG. 2. Different ways to create uniaxial anisotropy profiles in the device. (a) A cartoon schematic of the device creating the desired PMA profile via inducing voltage on the electrode gate through an insulator. This creates a concentric-like uniaxial anisotropy profile. (b) He^+ ion irradiation can also be used to modify the magnetic properties of magnetic ultrathin films by using a focused ion beam, these magnetic properties can be changed at the nanometer scale to pattern magnetic tracks as required.

two different uniaxial anisotropy profiles: a spiral-like uniaxial anisotropy profile for a 5-bit synapse, as shown in Fig.1(d); and three concentric-like uniaxial anisotropy profiles for a 4-bit, 5-bit, and 6-bit synapse as shown in Fig.1(e,f) respectively. Skyrmion lattice is generated in all four devices using a current pulse of value 10^4MA/m^2 for a duration of 2ns that is spin-polarized in $+z$ direction, skyrmions are locally injected in the FM layer along the periphery and at the center of the device. The skyrmion lattice consisting of $16+1$ skyrmion is relaxed for 5ns, $32+1$ skyrmion relaxed for 1ns, and $64+1$ skyrmion relaxed for 10ns after the local injection in the FM layer to enable a stable motion of the skyrmion lattice. The device description of our proposed devices is as follows: In a 32-state, 5-bit skyrmionic synapse based on a spiral uniaxial anisotropy profile, with a diameter of 500nm and height of 0.5nm. The device radius is 250nm while the detector region is of radius 150nm. The spiral Ku track passage is 30nm wide with a 10nm thickness band having a high uniaxial anisotropy value of 1MJ/m^3 .

Similarly, for 16, 32 and 64-state skyrmionic synapses based on a concentric uniaxial anisotropy profile, the device dimensions along with device radius, detector radius, Ku track passage, Ku track passage thickness with their corresponding high uniaxial anisotropy values are denoted by R_{device} , R_{detector} , $Ku \text{ track}_{\text{spacing}}$, $Ku \text{ track}_{\text{thickness}}$ & Ku_{high} respectively in I.

Fig.1 shows the locally injected skyrmion lattice in the FM layer of the device for the case of 16, 32 and 64 states where the z-component of the normalized magnetization (i.e., m_z in the x-y plane) is color-coded and the color bar shows its magnitude. Skyrmions in thin films and multi-layers experience a transverse deflection subjected to a gyrotropic force when moving or driven by the spin current called the skyrmion

TABLE I. The Synapse device parameters

| Bit | No. of states | Profile | Dimension | R_{device} | R_{detector} | Ku track _{spacing} | Ku track _{thickness} | Ku_{high} |
|-----|---------------|------------|-----------------------|---------------------|-----------------------|-----------------------------|-------------------------------|--------------------|
| 4 | 16 | Concentric | 330nm x 330nm x 0.5nm | 165nm | 110nm | 20nm | 5nm | 1.0 MJ/ m^3 |
| 5 | 32 | spiral | 500nm x 500nm x 0.5nm | 250nm | 150nm | 30nm | 10nm | 1.0 MJ/ m^3 |
| 5 | 32 | Concentric | 500nm x 500nm x 0.5nm | 250nm | 180nm | 30nm | 5nm | 1.2 MJ/ m^3 |
| 6 | 64 | Concentric | 650nm x 650nm x 0.5nm | 325nm | 220nm | 30nm | 5nm | 1.2 MJ/ m^3 |

hall effect(SkHE). Our device design benefits from the Skymion hall effect(SkHE), which is usually disregarded due to annihilation issues.

To move the skyrmion lattice, a current perpendicular to the plane (CPP) generates a spin-polarized current that makes the skyrmion lattice excited to a steady state of persistent circular trajectory but is directed towards the constricted spiral or concentric-like profile in unison along the boundary created by high Ku nano-track followed by a trail of skyrmions. At the spiral or concentric opening the skyrmions not only experience edge repulsion but also a self-directional repulsive force that guides the trail of skyrmions towards the nano track created by the bounded high Ku tracks or rings. The applied spin-polarised current results in spin torque acting on the FM layer, where the spin polarisation takes the form of a vortex-like state from the in-plane('write' current: Terminal T3 to T1) magnetized reference layer. The vortex-like magnetic configuration with a radial magnetization configuration is set at a polarization angle of 180° (e.g., $\Psi = 180^\circ$) [26, 27] which simulates the polarization vector through the relation $m_{RL} = (\cos\Phi_p, \sin\Phi_p, 0)$, where $\Phi_p = \tan^{-1}y/x + \Psi$ and (x, y) are spatial coordinates in the film plane with origin being at the center of the nanodisk.

When an electrical current is injected along the +z-direction into the system, the spin current drives the skyrmion into a clockwise gyration towards the center but as it encounters the high Ku passage, it starts to move along the track until the duration of the current pulse. However, at the center of the disk, it encounters an already pinned skyrmion which does not let the incoming skyrmions get pinned at the center but repels them. Now, the current pulse is switched along -z-direction and the skyrmion lattice is driven towards the edge again following the same constricted high Ku path and eventually reaching a steady state of anti-clockwise gyration along the edge of the disk. This periodic motion of the skyrmion in the nano-disk can be used as a synapse.

The area where these high Ku constricted tracks are created is used as a detector region forming the post-synapse region where the linearly increasing number of skyrmions during the positive current pulse results in LTP. While the linearly decreasing number of skyrmions at a negative current pulse results in LTD. The MTJ (detector)[28] employed in the post-synapse region reads out the magneto resistance[29], along the 'read' path

between terminal T2 to T1, and a range of conductance values corresponding to the applied current pulse train is obtained as synaptic weights. The linear change in conductance with the number of skyrmions is shown in Fig.6(a,b).

However, when the current density magnitude exceeds $2.5\text{MA}/\text{cm}^2$, few skyrmions can be annihilated either at the center or the edge of the nano-disk due to an increased Magnus force with the increasing current. Still, a linear profile is maintained even at an increasing current density. Also, If the center pinned skyrmion is not present, the incoming skyrmions near the center are pushed by the current in the high Ku region, which in turn provides a repulsive force resulting in reduced skyrmion size and hence, the skyrmion vanishes. Thus, the center pinning of a skyrmion holds importance in the device design.

The spiral or concentric-shaped constricted Ku profiles can be obtained using He ion irradiation techniques[30, 31] which provide the desired profile without getting into the complexity of VCMA [32] methods for modifying anisotropy as shown in Fig.2(a,b). The high uniaxial anisotropy track thickness and value are chosen such that the skyrmions don't crossover them but instead align along the narrow tracks. The concentric Ku profile devices have openings along 180° with a slightly lower opening at the start having an inclined L-shaped wedge to avoid skyrmion dodging at the entry supporting the skyrmion trajectory.

Additionally, for a 64-state skyrmionic synapse device a high Ku outer ring(radius:285nm (Fig.1f)) is introduced which helps in accommodating more skyrmions in a compact space or smaller geometry. The inner ring skyrmions enter the post-synapse region followed by the outer ring skyrmions. The spiral-like profile has an opening on the right side along 180° supporting the skyrmion trajectory. If the skyrmions reach the innermost track they might annihilate in the high Ku region near or at the center due to the experienced forces. The more preferred Uniaxial anisotropy profile is the one with concentric Ku rings because of two reasons: 1) the skyrmion coming in the innermost ring can circle the center-pinned skyrmion without getting annihilated. 2)The total duration of device operation is reduced, as explained in the results and discussion section of the paper.

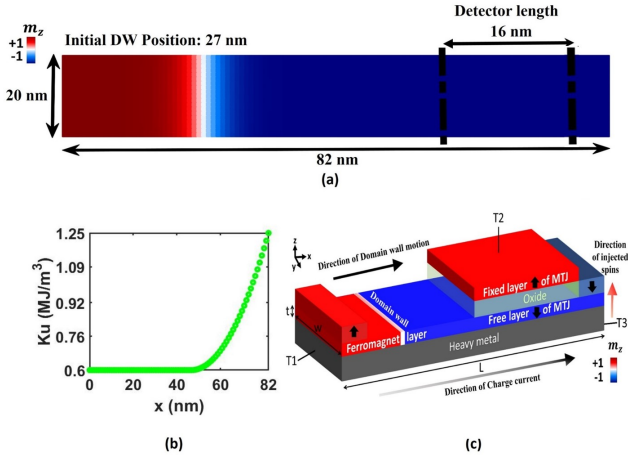


FIG. 3. Domain wall-based ReLU device (a) 2D view of the domain wall track for the ReLU device (b) The plot for applied parabolic uniaxial anisotropy profile (PMA) along the length of the device. (c) 3D view of the domain wall device in ReLU circuit

C. Domain wall-based ReLU device

The proposed domain wall ReLU (Rectified Linear Unit) device consists of a SOT-based monolayer FM (82nm) with a single domain wall and a CMOS-inverter circuit as shown in Fig.4a. The ferromagnet layer exhibits a perpendicular magnetic anisotropy (PMA) with oppositely polarized transverse magnetic regions separated by a domain wall. The device has a parabolic uniaxial anisotropy profile in the FM layer that can be achieved [30, 33] using oxidation (under oxidation, oxidation, & over oxidation) of the FM layer under positive bias voltage. The Uniaxial anisotropy profile of the FM layer is constant in the left section from 0nm to 47nm and is parabolic in the other section from 47 nm to 82 nm as shown in Fig.3(b). The spin-orbit coupling at the FM-HM interface leads to the Dzyaloshinskii-Moriya exchange interaction (DMI) resulting in a stable Neel domain wall (DW). The strong DMI not only rotates the DW moment but also tilts the DW line profile in the x-y axis due to the energy minimization principles reported in [34, 35]. The domain wall in the ferromagnet layer is driven by an electrical charge current (Terminal T1 to T3) passed through the HM layer in the x-direction giving rise to a spin-polarized current flowing in the +z-direction, having spins that are oriented along the -y-direction with a parabolic anisotropy variation under the detector region. The FM length is 82nm with a width of 20nm [36] and thickness of 1nm as shown in Fig.3(a). For the heavy metal, a gold-platinum alloy ($\text{Au}_{0.25}\text{Pt}_{0.75}$) has been chosen over the standard platinum (Pt) metal layer to enhance power efficiency at the device level [25, 37].

The domain wall read-out [38] is done using an MTJ from 'read' terminal T2 to T3. A range of conductance values corresponding to the varying domain wall posi-

tions is obtained for the varied current range. The fixed layer with magnetization in the +z direction along with the oxide and the free layer forms the MTJ (Fig.3c). The ferromagnet layer forms the free layer of the MTJ whose magnetization is altered by introducing the domain wall driven by spin-orbit torque.

The detector is strategically placed at a distance of 63nm to 79nm within the structure such that the domain wall position shows a significant monotonic step-wise increase with respect to the applied current density. This placement allows for the implementation of ReLU-like functionality by our proposed device incorporating linearity for domain wall positions under the MTJ and non-linearity by introducing zero otherwise. A fixed magnetization layer is used at the ends of the ferromagnet layer with an antiferromagnetic layer above to create an exchange bias that pins the magnetization at the ends of the wire, ensuring domain wall stabilization. Thus, protecting it from getting destroyed at the edges [39, 40]. Spin-orbit torque (SOT) is preferred over Spin-Transfer Torque (STT) for domain wall motion due to its faster settling time and lower current requirements for the same operation [41–43].

Fig.4a depicts the in-plane current I_{charge} as the varying input that manipulates the domain wall positions in the FM layer. While the bias current I_b shifts the output such that the CMOS-domain wall hybrid circuit simulates the ReLU output. The corresponding resistance values obtained from the conductance measurement are connected to a resistor (R_1) and then fed through a voltage divider circuit to a CMOS inverter. The output across the voltage divider drives the CMOS inverter pair in the linear region. Thus, facilitating the ReLU output to be implemented as a ReLU module (Fig.4a) for both activation and max-pooling (Fig.4b) functionality in the CNN.

D. Max Pooling

The CNN (Fig.9) has four major layers: The convolutional layer, the ReLU layer, the pooling layer, and the fully connected layer. The convolutional layer is implemented using crossbar arrays connected via the

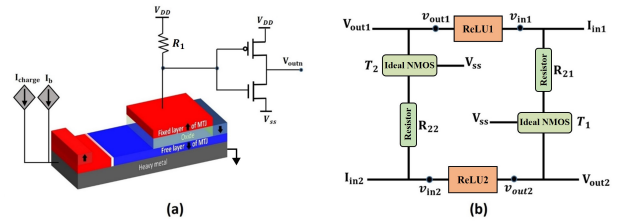


FIG. 4. Domain wall-based ReLU device (a) CMOS-domain wall-based hybrid ReLU circuit (b) 2-Input ReLU Max Pooled circuit connection

TABLE II. The micromagnetic simulation parameters for the synapse device

| Symbol | Parameters | value |
|-------------|-----------------------------|----------------------|
| M_s | Saturation magnetization | 580KA/m |
| α | Gilbert damping factor | 0.3 |
| D | DMI constant | 3mJ/m ² |
| A_{intra} | Exchange stiffness constant | 15pJ/m |
| P | Spin polarization factor | 0.4 |
| K_u | PMA constant | 0.8MJ/m ³ |

spintronic device, such as the skyrmionic synapse device in our case(II B). The output from the convolutional layer serves as an input to the activation or the ReLU layer, which is implemented using the SOT-based CMOS-Domain wall hybrid circuit(II C).

After the feature extraction stage, the max-pooling layer is implemented by linking the individual ReLU circuits in a specific design such that the ‘‘winner takes all’’. This computational principle stems from the interconnect and ReLU connection creating competition among the interconnected ReLU circuits such that only one of them corresponds to the maximum input, and others settle at zero. The interconnect consists of a resistor connected to an NMOS transistor whose gate terminal is connected to the output of other ReLU circuits. The output drawn from one ReLU circuit is dependent on the output voltage of another ReLU circuit. As a result of the competition, a negative current is injected into all other ReLU devices by the ReLU circuit with non-zero output at the end of the max pooling operation.

Fig.4(b) shows ReLU plus max pooling function being simultaneously performed for two inputs. We performed a simultaneous ReLU plus max pooling for 9 Inputs which are summed without the boundation of identifying the circuit with the maximum input. Supplementary details of a similar circuit with ReLU plus max-pooling can be found in [44].

III. SIMULATION METHODS

The micro-magnetic simulations for the synapse are performed using OOMMF[45] with the added DMI extension module. The dimensions of the synaptic devices are mentioned in Table (I) with discretization of 2 nm x 2 nm x 0.5 nm. The proposed synapse devices are simulated using the parameters mentioned in II for the Co-Pt system[46].

The micro-magnetic simulations for the domain wall-based ReLU are performed on a GPU-accelerated numerical package (mumax3). The domain wall device has a thickness of 1nm with lateral dimensions 82nm x 20nm. The cell size is 1 nm x 1 nm x 1 nm. The proposed domain wall is simulated using the matching parameters mentioned in III for the Co – Au₂₅Pt₇₅ system[47]. The uniaxial anisotropy for the device length 0 to 47nm remains

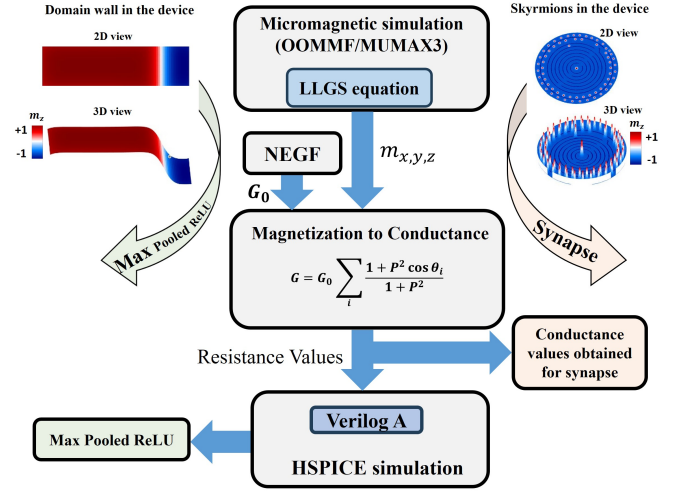


FIG. 5. Simulation methodology

constant at $Ku_c = 0.6MJ/m^3$. The profile varies parabolically for the device length 47nm to 82nm with the relation $Ku = Ku_c + 530.6122 * (i - 47)^2$ where i varies from 47 to 82 representing distinct regions, as per the mumax3 code.

The hybrid device circuit for ReLU-Max pooling is simulated in HSPICE using Verilog A. The proposed circuit parameters are mentioned in III.

A schematic overview of the simulation methodology is shown in Fig.5, A detailed explanation for both skyrmion and domain wall devices is mentioned below in subsections A, B, C, D, and E.

A. Micromagnetic simulation framework for the skyrmion-based synapse device

The magnetization dynamics for CPP are computed using the Landau-Lifshitz-Gilbert (LLG) equation with the Slonczewski spin transfer torque(STT) is defined as:

$$\frac{d\mathbf{m}}{dt} = -|\gamma|\mathbf{m} \times \mathbf{H}_{eff} + \alpha \left(\mathbf{m} \times \frac{d\mathbf{m}}{dt} \right) + |\gamma|\beta_j \epsilon (\mathbf{m} \times \mathbf{m}_{RL} \times \mathbf{m}) - |\gamma|\beta_j \epsilon' (\mathbf{m} \times \mathbf{m}_{RL}) \quad (1)$$

where, $\gamma = 2.211 \times 10^5$ m/(A.s) is the gyromagnetic ratio, \mathbf{m}_{RL} is the magnetization of RL, $\beta_j = \hbar J / (\mu_0 e t_z M_s)$, $\epsilon = \frac{P\Lambda^2}{(\Lambda^2+1)+(\Lambda^2-1)\cdot(\mathbf{m}\cdot\mathbf{m}_{RL})}$, and ϵ' is the secondary spin transfer term. we have set $\Lambda=1$, and the secondary spin transfer term $\epsilon'=0$ to remove the dependence of ϵ on $m\cdot m_{RL}$ and the field like out of plane torque respectively in all simulations.

Here \hbar , e , t , P , and J are reduced Planck’s constant, electronic charge, thickness of the FM layer, polarization, and current density, respectively. The effective magnetic

TABLE III. The simulation parameters for Domain wall-based ReLU Max Pooled device

| Symbol | Parameters | value |
|------------------|---|---------------------|
| M_s | Saturation magnetization | 580KA/m |
| α | Gilbert damping factor | 0.3 |
| D | DMI constant | 3mJ/m ² |
| A_{intra} | Exchange stiffness constant | 15pJ/m |
| P | Spin polarization factor | 0.15 |
| ξ | $\frac{ field-liketorque }{ damping-liketorque }$ | -2 |
| θ | Spin Hall Angle | 0.3 |
| R_{HM} | Resistance of HM | 850.75 Ω |
| ρ_{HM} | resistivity of HM | 83 $\mu\Omega cm$ |
| t_{HM} | Thickness of HM | 4nm |
| L_{HM}, W_{HM} | length, Width of HM | 82nm, 20nm |
| L, W | Length, Width | 82nm, 20nm |
| V | Volume of FM | 1640nm ³ |
| C_{MTJ} | MTJ Capacitance | 26.562aF |
| R_1 | Reference Resistor | 58.954K Ω |
| R_{21} | Resistor in NMOS current source | 42K Ω |
| I_b | Biasing current | 39.735uA |
| V_{DD}, V_{SS} | Voltage sources | 0.5V, -0.5V |
| Δ_t | Simulation time step | 0.05ps |

field \mathbf{H}_{eff} in relation to local magnetization is given by:

$$\mathbf{H}_{eff} = -\frac{1}{\mu_0 M_s} \frac{\delta E}{\delta \mathbf{m}} \quad (2)$$

where μ_0 is the space permeability and E is the total energy given as follows:

$$E = \int dV [A(\nabla \mathbf{m})^2 + \varepsilon_{DMI} + K_u [1 - (\mathbf{m} \cdot \mathbf{z})^2] - \frac{\mu_0}{2} \mathbf{m} \cdot \mathbf{H}_d] \quad (3)$$

where the first term is the exchange energy with the exchange stiffness constant A, the second term is an interfacial form of DMI resulting in a Neel skyrmion $\varepsilon_{DMI} = D \left(m_z \frac{\partial m_x}{\partial x} - m_x \frac{\partial m_z}{\partial x} + m_z \frac{\partial m_y}{\partial y} - m_y \frac{\partial m_z}{\partial y} \right)$ The third term defines the uniaxial anisotropy energy with the anisotropy constant K_u , and the demagnetization field forms the last term.

B. Skyrmion dynamics

The Skyrmion dynamics in the free FM layer controlled by the spin current is described by the Thiele equation :

$$\mathbf{G} \times \mathbf{v} - \alpha \mu_0 M_s t_z \mathbf{v} \cdot \mathbf{d} / \gamma + \mathbf{F}_{STT} + \mathbf{F} = 0 \quad (4)$$

The first term is the Magnus force with the velocity of skyrmion and the gyrovector \mathbf{G} . The second term describes the dissipative force with the damping α and the dissipative tensor $\mathbf{d} = \begin{pmatrix} d & 0 \\ 0 & d \end{pmatrix}$, where

$d = \frac{1}{4\pi} \int dx dy (\partial_x \mathbf{m} \cdot \partial_x \mathbf{m})$. The third term represents current-induced driving force due to the spin transfer torque, which can be decomposed into two orthogonal directions (the radial \hat{r} and the tangential direction \hat{t} in the polar coordinates), $\mathbf{F}_{STT} = F_r \hat{r} + F_t \hat{t}$, the component F_i where (i=r or t) is given by $F_i = -\mu_0 \beta_j M_s t_z \int dx dy [(\mathbf{m} \times \mathbf{m}_p) \cdot \partial_i \mathbf{m}]$, where β_j is the applied vertical current density. The last term is the boundary-induced force which includes edge repulsion, the nearest neighbor skyrmion repulsion forces, and little effect of the high uniaxial anisotropy outer ring (only in the case of 6-bit skyrmionic synapse) when the skyrmion moves steadily in the nanodisk (means radial part of the velocity is zero). Therefore equation 4 can be written as :

$$v_t G + F_r + F = 0 \quad (5)$$

$$\alpha \mu_0 M_s t_z v_t d / \gamma + F_t = 0 \quad (6)$$

From the above two equations, we deduce that the steady motion of skyrmion in the nanodisk requires a balance between the Magnus force and the boundary force. Thus, the skyrmion lattice will move toward the center of the nanodisk at the positive current pulse train and away from the center on the application of a negative pulse train.

C. Micromagnetic simulation framework for Domain wall-based ReLU device

The methodology for micromagnetic modeling of the magnetization dynamics in spin-orbit-torque driven domain wall is reported in Ref. [48]. The GPU-accelerated micromagnetic package mumax3 uses custom field functionality to implement spin-orbit torque (SOT) with the Landau-Lifshitz-Gilbert (LLG) equation given as:

$$\frac{d\mathbf{m}}{dt} = -|\gamma| \mathbf{m} \times (\mathbf{H}_{eff} + \mathbf{H}_{ST}) + \alpha \left(\mathbf{m} \times \frac{d\mathbf{m}}{dt} \right) \quad (7)$$

where H_{eff} is the effective field and H_{ST} is the spin torque consisting of the damping-like and the field-like term.

$$\mathbf{H}_{ST} = a_J \mathbf{m} \times \mathbf{p} + b_J \mathbf{p} \quad (8)$$

where the unit vector \mathbf{p} characterizes the direction of the spin-polarization. The a_J , b_J , and ξ ($\xi = b_J / a_J$) are the magnitudes of the damping-like, field-like terms and the ratio of the field-like term and damping-like term respectively. The spin current from the heavy metal layer is given by Hirsch[49], Takahashi, and Maekawa[50]

$$I_s = \theta \frac{l_{FM}}{t_{HM}} I_c \times \mathbf{P} \quad (9)$$

Where I_s , θ , l_{FM} , t_{HM} , I_c , and \mathbf{P} are the magnitude of spin current, spin Hall angle, length of the FM, thickness of

the HM layer, charge current and polarization of the spin current respectively. A charge current in the +x direction injects a y-polarised spin current in the FM layer in the z-direction, inducing domain wall motion along the device length. The resistance of the HM is given by $R = \rho_{\text{HM}}/W_{\text{HM}}t_{\text{HM}}$, where ρ is the resistivity of HM(Au_{0.25}Pt_{0.75}), l_{HM} is the length of HM, W_{HM} is the width of HM and t_{HM} is the thickness of HM.

D. Electrical read out

When all the skyrmions(domain wall) reach the detector region, The TMR calculation is done by a differential method, considering that the whole magnetic tunnel junction (MTJ)device consists of many 2 nm × 2 nm (1nm x 1nm) uniform cells in the xy plane [51]. The conductance of each cell is obtained by the extended Julliere's model[52, 53] and slonczewski conductance model[54] which can be shown as:

$$G = G_0 \sum_i \left(\frac{1 + P^2 \cos\theta}{1 + P^2} \right) \quad (10)$$

NEGF is used to calculate the G_0 , where G_0 is the conductance when the magnetization is perfectly parallel to the reference layer, P is the spin polarization which is set to be 0.4 in our simulation, and θ is the magnetization of each cell with respect to the reference layer.

The conductance obtained is then converted into weights on a normalized scale using the relation:

$$Weight = \frac{G - G_{min}}{G_{max} - G_{min}} \quad (11)$$

Here $G_{max}(G_{min})$ is the maximum (minimum) conductance of the synapse. We further calculated the write resistance R_{Write} of our proposed device using the Valet and Fert model[55, 56] for a Bilayer structure consisting of ferromagnet layers(resistivity(ρ_F^*), thickness(t_F), $\beta_F \neq 0$) and the non-magnetic layer($\rho_{N1}^*, \rho_{N2}^*, t_{N1}, t_{N2}$) under the case of spin-flip length $l_{sf}^{F,N1,N2} \gg t_F, t_{N1}, t_{N2}$:

$$Area * R_{write} = r_0 + r_{SI}(\theta) \quad (12)$$

$$r_{SI}(\theta) = r_{SI}^P + (r_{SI}^{AP} - r_{SI}^P) \frac{(1 - \cos(\theta))}{2} \quad (13)$$

$$r_0 = 2\rho_f^* t_F + \rho_{N1}^* t_{N1} + \rho_{N2}^* t_{N2} \quad (14)$$

$$r_{SI}^{AP} = 2\rho_f^* t_F + \rho_{N1}^* t_{N1} + \rho_{N2}^* t_{N2} + 2r_b^{F/N1} + 2r_b^{F/N2} \quad (15)$$

$$\begin{aligned} (r_{SI})^P &= r_{SI}^{AP} - (\beta_F \rho_f^* \frac{t_F}{t_F + t_{N1}} L_1 \\ &+ \beta_F \rho_f^* \frac{t_F}{t_F + t_{N2}} L_2 \\ &+ 2r_b^{F/N1} \Gamma^{F/N1} + 2r_b^{F/N2} \Gamma^{F/N2}) / r_{SI}^{AP} \end{aligned}$$

where r_0 is the resistance of the nonmagnetic layer in series with a magnetic one, $r_{SI}(\theta)$ is the spin-coupled interfacial resistance accounting for the angular dependence[57] of the RL and free FM layer with $\theta = 90^\circ$ in Eq 12 & 13. The spin-coupled interfacial resistance for Parallel(Anti-parallel)($r_{SI}^{P,AP}$) configuration is defined in Eq 15 & 16. The resistivity of the Ferromagnet and non-magnetic layer is $\rho_F^* = \rho_F / (1 - \beta_F^2)$ and $\rho_N^* = \rho_N$ respectively. The $r_b^{F/N1}$ and $r_b^{F/N2}$ are the interface resistances between the Co/Pt and Ru/Co. The $L_i = t_F + t_{Ni}$, where $i=1,2$. While the bulk and interfacial spin asymmetry coefficient is defined as β_F & $\Gamma^{F/N1,F/N2}$.

The parameter values used for the resistance calculation are mentioned in IV. The energy consumption required to move the skyrmions in the nano tracks for hardware implementation in the neural network is calculated using:

$$E_{write} = I_c^2 R_{write} \Delta \quad (16)$$

Here, E_{write} is the Energy dissipated per weight update, I_c is the charge current, and Δ is the length of write pulse required to change the weight of our synapse device to move each skyrmion from the pre-synapse region to the post-synapse region calculating the energy consumption per weight update.

E. HSPICE using Verilog A

The obtained resistance values from the electrical read-out as described in III D are utilized in the circuit-level simulation of the ReLU max-pooling circuit using Verilog A. In the HSPICE simulation of a single ReLU, the obtained resistance values act as a variable resistor connected to a constant resistor (R_1) of value 58.954K Ω , creating a voltage divider. The output from the divider is fed as an input to the CMOS inverter pair based on the 16nm node of the predictive technology model(PTM). A 9-input interconnection of such ReLU circuits with an interconnect network consisting of resistors and NMOS transistors is implemented in HSPICE to obtain the combined result of the ReLU-max pool function.

IV. RESULTS AND DISCUSSION

we first describe the synapse device followed by the CMOS hybrid domain wall-based ReLU Maxpool device.

As described in IIB and III, all four skyrmionic synapse devices are simulated. The FM layer in contact with the HM (gives rise to DMI at the FM/HM interface) forms the nano track for our proposed devices with either spiral or concentric-like uniaxial anisotropy profiles. A circular detector(MTJ) region of reduced radius as shown in Fig.1(b,c) is formed by sandwiching the oxide layer between the FM and the free FM layer, forming the post-synapse region of our synaptic device. The area between

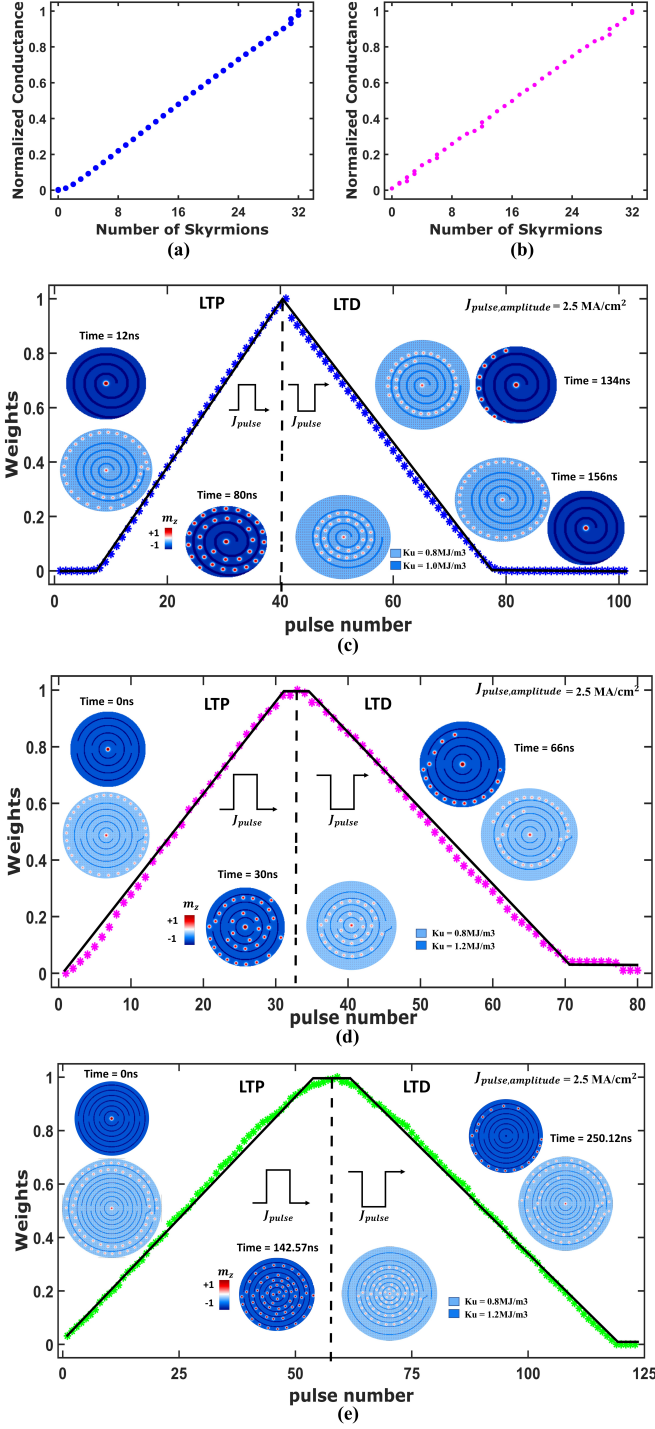


FIG. 6. Plot for Normalized conductance versus the number of skyrmions in the post-synapse region (a) For a 5-bit synaptic device with spiral uniaxial anisotropy profile. (b) for a 5-bit synaptic device with concentric-like uniaxial anisotropy profile. The plot of synaptic weight versus pulse number during LTP and LTD with snapshots of micro-magnetic simulations showing m_z , for the full device and the post-synaptic region at different time stamps (c) for 5-bit skyrmionic synapse with spiral uniaxial anisotropy profile (d) for 5-bit skyrmionic synapse with concentric uniaxial anisotropy profile. (e) 6-bit skyrmionic synapse with concentric uniaxial anisotropy profile.

TABLE IV. The parameters for energy consumption per weight update in our proposed synapse devices

| Symbol | Parameters | value |
|------------------|--|---|
| ρ_{Co} | Resistivity of FM(Co) | $19\mu\Omega cm$ [58] |
| ρ_{Pt} | Resistivity of NM(Pt) | $100\mu\Omega cm$ [59] |
| ρ_{Ru} | Resistivity of NM(Ru) | $18\mu\Omega cm$ [60] |
| t_{Co} | Thickness of FM(Co) | 0.5nm |
| t_{Pt} | Thickness of NM_1 (Pt) | 0.5nm |
| t_{Ru} | Thickness of NM_2 (Ru) | 7nm [60] |
| l_{sf}^{Co} | Spin flip length of FM | 60nm [61] |
| l_{sf}^{Pt} | Spin flip length of NM_1 | 0.5nm-14nm [61] |
| l_{sf}^{Ru} | Spin flip length of NM_2 | 14nm [62] |
| $r_b^{Co/Pt}$ | Interface resistance of FM/ NM_1 | $1.7 \pm 0.25 \text{ f}\Omega m^2$ [63] |
| $r_b^{Co/Ru}$ | Interface resistance of FM/ NM_2 | $0.5 \text{ f}\Omega m^2$ [62] |
| β_{Co} | Bulk spin asymmetry coefficient of FM | 0.46 [63] |
| $\Gamma_{Co/Pt}$ | Interfacial spin asymmetry coefficient of NM_1 | 0.38 ± 0.06 [63] |
| $\Gamma_{Co/Ru}$ | Interfacial spin asymmetry coefficient of NM_2 | -0.2 [62] |

the circumference of the nanodisk and the detector forms the pre-synapse region where the skyrmions are nucleated in a stable form such that the skyrmion-skyrmion repulsion aids in the skyrmion motion on current application in the device.

In the 5-bit (concentric-like Ku profile) and 5-bit (spiral and concentric-like profile), the skyrmions are placed in the presynapse region along the circumference, see snapshot in Fig.1(d,e) but in the 6-bit (concentric-like Ku profile) (Fig.1f), a two-line concentric formation of the skyrmions along the circumference separated by an additional high Ku ring of value 1.2 MJ/m^3 and 5nm thickness. Fig.1(f) shows a small opening in the outer ring which supplies further skyrmions to the post-synapse region via the inner ring. This outer ring enables more skyrmion accommodation in a diameter of 650nm with 64 skyrmions compared to the inner diameter of 500nm accommodating 32 skyrmions. If we place the 64 skyrmions in a concentric formation without the outer separation ring, the outer skyrmions will push the inner skyrmions toward the high Ku regions under the detector. This can cause skyrmion annihilation due to the push and pull experienced by the presence of high Ku repulsion, edge repulsion, and neighboring skyrmion repulsion resulting

in reduced size and finally vanishing under the influence of applied current.

As shown in Fig.1(f), high K_u value i.e., the uniaxial anisotropy is depicted in the shade of dark blue for both the track and the outer ring. The FM layer of the nanodisk forms the free layer of the MTJ having an opposite magnetization to the fixed FM (m_z : red) layer.

As the skyrmions start to move under the influence of the current pulse the magnetization of the free layer of the MTJ (FM) changes accordingly. This can be electrically read using magnetoresistance. The conductance value from magnetization is obtained as explained in IIID. When no skyrmions are present under the MTJ, the conductance value corresponds to G_{\min} , the lowest conductance. When all the skyrmions move under the MTJ, the conductance value corresponds to G_{\max} , the maximum conductance. The applied current density with spin polarisation (according to the m_{RL}) injected in the FM varies the conductance of the device as a trail of skyrmions reaches the detector region. This results in a linear weight variation as explained in IIID. Fig.6(a,b) shows a linear relation between the vertical axis representing normalized conductance or weights versus the horizontal axis representing the number of skyrmions, which is an effect of the magnetic moment alignment of the center of the skyrmion with the fixed FM layer of the detector.

Now we investigate our simulated devices using identical current pulses with spin polarisation according to the m_{RL} applied into the FM based on the artificial synapse operations. The synapse operation consists of initiation, potentiation(LTP), and Depression(LTD) analogous to the persistent strengthening or weakening of synapse connections as plotted and marked in Fig.6(a,b) with the vertical axis representing the weights and the horizontal axis as the pulse number. The synapse can also have short-term plasticity(STP) which is a constant state between the LTP and LTD slopes or short-term change that decays over tens of ms or minutes.

The Energy calculations are done as per Eq(16), as described in IIID. For a charge current of 2.1 mA and Δ of 2ns corresponds to $E_{\text{write}} = 0.8724$ fJ/unit for the 4-bit skyrmionic synapse having a concentric Ku profile. For a charge current of 4.9 mA and Δ of 2ns corresponds to $E_{\text{write}} = 2.0028$ fJ/unit for both 5-bit skyrmionic synapses having a concentric and spiral Ku profile. For a charge current of 8.3 mA and Δ of 2.5 ns corresponds to $E_{\text{write}} = 4.2309$ fJ/unit for 6-bit skyrmionic synapses having a concentric Ku profile.

In the next subsections, a detailed working of each profile with an applied pulse train is studied.

A. Synapse based on spiral Ku profile

After the skyrmions are locally injected and relaxed as shown in Fig.6(c), full device snapshots (light blue) with color-coded Ku and m_z are shown at different simulation

time stamps along with the post-synapse or detector region of the device (in dark blue color). The current pulse of value $J= 2.5\text{MA}/\text{cm}^2$ at a pulse width of 1.5ns and period of 2ns is applied for a total duration of 186.15ns.

In the initiation process, the skyrmions are brought near the detector region for a duration of 16ns. The snapshot in Fig.6(c) shows no skyrmion under the detector at time= 12ns but several skyrmions can be seen inside the spiral opening which is not a part of the detector region. The detector starts at 150nm from the center.

For the LTP operation, a positive pulse train starts moving the skyrmion in the clockwise direction and the skyrmions start to enter the detector region one by one at each current pulse. The LTP operation takes place from 16ns to 80ns, where we observe a linear increase in weights, with G_{\max} corresponding to all the skyrmions under the detector region as shown in the snapshot at $t=80\text{ns}$.

For the LTD operation, a negative current pulse train starts moving the skyrmion in an anti-clockwise direction forcing skyrmions to move out of the spiral, corresponding to each pulse. Thus, linearly decreasing the weights as shown in the snapshot at $t=134\text{ns}$ with 8+1 skyrmions under the detector region. The LTD operation takes place from 80ns to 154ns. After which the device takes 154ns to 186ns(pulse number 93) for a complete reset. As shown at time $t=156\text{ns}$, there are no skyrmions under the detector and the device has obtained G_{\min} value. Thus, we could achieve linear and symmetrical LTP and LTD curves for our proposed geometry of a 5-bit (spiral-like Ku) synapse.

B. Synapse based on concentric Ku profile

Here, the initiation and reset time of the device is shorter as compared to that of the spiral-like Ku profile device. This happens because the skyrmions are present near the vicinity of the detector region. For the same 5-bit(concentric-like Ku) synapse, the initiation time, potentiation, and depression time are 2ns, 2ns to 60ns, and 66ns to 158ns respectively. As shown in Fig.6(d) at $t=0\text{ns}$, no skyrmions are present in the detector region representing minimum conductance G_{\min} . On a positive current pulse train application, the weights start to increase linearly(LTP) and attain the maximum at $t=60\text{ns}$, all the skyrmions are under the MTJ region corresponding to maximum conductance G_{\max} . here, we also observe STP for 60ns to 66ns. The LTD begins with the application of negative current application, moving the skyrmions out of the constricted concentric paths as shown at $t=102\text{ns}$, 16 skyrmions are out of the detector region. The applied current pulse train of $J=2.5\text{MA}/\text{cm}^2$ at pulse width and period of 1.86ns and 2ns respectively achieve the synapse operations in a total duration of 158ns(pulse number 79) including LTP, LTD, and STP.

Similarly, for a 4-bit(concentric-like Ku) synapse cur-

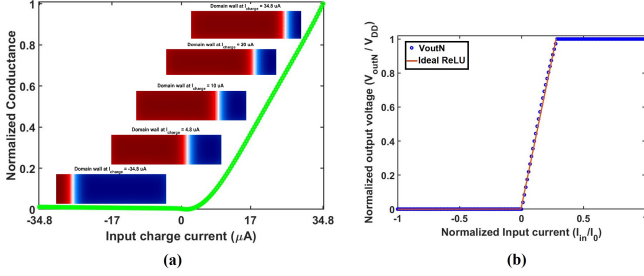


FIG. 7. Domain wall-based ReLU device (a) The plot for normalized conductance versus input charge current with snapshots of the domain wall at different input charge current (b) The plot for the ReLU function obtained using CMOS hybrid domain wall device .

rent density of $J=2.5\text{MA}/\text{cm}^2$ at pulse width and period of 1.8ns and 2ns respectively can achieve initiation, LTP, STP, LTD, and reset of the device in 20ns,20ns to 32ns,32ns to 34ns, 34ns to 72ns and 72ns to 80ns respectively in a total duration of 80ns for all synapse operations.

For a 6-bit(concentric-like Ku) synapse current density of $J=2.5\text{MA}/\text{cm}^2$ at pulse width and period of 2.2ns and 2.5ns respectively can achieve initiation, LTP, STP, LTD, and reset of the device in 25ns,25ns to 142.57ns,142.57ns to 147.6ns, 147.6ns to 297.6ns and 297.6ns to 305ns respectively in a total duration of 305ns(pulse number 122) for all synapse operations. The snapshots in Fig.6(e) at $t=0\text{ns}$ correspond to minimum conductance G_{min} and $t=142.57$ correspond to the maximum conductance G_{max} . At $t=250.12\text{ns}$, LTD operation has already set in with 44 skyrmions being moved out of the detector heralding the reset position of the device.

C. ReLU and Max Pooling function based on the domain wall

As described in II(C,D) and III, the domain wall-based ReLU device is implemented. The domain wall, initially placed at 27nm is relaxed and supplied with a varying electrical charge current in the range $-34.8\mu A$ to $34.8\mu A$. As the SOT-driven domain wall moves along the nano track it encounters an increasing parabolic uniaxial anisotropy profile (Ku in the range $0.6\text{MJ}/\text{m}^3$ to $1.25\text{MJ}/\text{m}^3$) which gradually slows down the domain wall velocity, making the velocity zero after some time. This operation allows us to implement the ReLU-like functionality in the device utilizing the linear variation of the conductance obtained under the MTJ for domain wall positions at a particular instant.

Fig.7(a) shows snapshots of domain wall positions on the FM nano track. The Domain wall reaches at position = 9nm (56.7nm) corresponding to an un-normalized

conductance value of $3.91\mu\Omega$ ($4.83\mu\Omega$) at $I_{charge} = 38.5\mu A$ ($4.8\mu A$), $Ku = 0.60\text{MJ}/\text{m}^3$ ($0.653\text{MJ}/\text{m}^3$) in 0.3ns(0.7ns). The conductance here is near to the G_{min} value($3.125\mu\Omega$), thus the graph is flat corresponding to the non-linearity part of the ReLU function that returns 0 value for any negative value. The linearity relation is observed after the domain wall reaches beyond 63nm under the detector region. The domain wall reaches 63.78nm with an un-normalized conductance value of $21.74\mu\Omega$ at $I_{charge} = 14\mu A$, $Ku = 0.753\text{MJ}/\text{m}^3$ in 0.3ns. Similarly, for $I_{charge} = 20\mu A$ ($34.8\mu A$) the domain wall reaches 65.8nm (71.88nm) with an un-normalized conductance value of $36.36\mu\Omega$ ($73.65\mu\Omega$) at $Ku = 0.7915\text{MJ}/\text{m}^3$ ($0.9316\text{MJ}/\text{m}^3$) in 0.3ns (0.2ns). The G_{max} (= $73.65\mu\Omega$) is obtained at $I_{charge} = 33.33\mu A$ after which the domain wall position is saturated due to the pinning of the edges which restricts the domain wall motion in the device between 3nm to 79nm.

If the domain wall pinning is not executed the domain wall will vanish beyond $I_{charge} = 36\mu A$. The SOT-driven domain wall device enables faster device reset in 1.3ns and the domain wall settles in 0.3 to 0.2 ns range. The obtained ReLU-like function is adjusted and aligned with a biasing current (I_b). The obtained conductance values are used as a variable resistor in the voltage divider circuit as shown in Fig.4(a).

Using HSPICE, embedding the information in Verilog A, an electrical read-out circuit is designed, and the variable resistor and a constant resistor ($58.954\text{K}\Omega$) form a voltage divider feeding a CMOS inverter pair. The output obtained from the inverter circuit forms the ReLU function. The obtained ReLU plot as shown in Fig.7(b) obtained from the CMOS hybrid domain wall device shows ReLU-like functionality in the range $-10.67\mu A$ to $10.67\mu A$. The power consumed by the single ReLU module is $4.7358\mu W$ which includes(Energy= 0.6484fJ) consumed by the domain wall device. A similar graph is also obtained after the max pooling circuit.

A specimen circuit of 2-Input ReLU- Max pooling is shown in Fig.4 (b). An interconnect network with an ideal NMOS and a resistor($R_{21} = R_{22}$) is attached to the ReLU circuit creating competition between the ReLU circuits as the input current drawn from ReLU1 depends on the output voltage of ReLU2. The gate of the NMOS transistor connects to both the ReLU's output. This design strategy creates competition calculating both the ReLU and max pooling function simultaneously. Fig.8 shows the transient response for a 9-Input ReLU Max Pooling network corresponding to a 3x3 pooling layer for 400 Monte Carlo simulations as the input current is varied using the Monte Carlo method.

V. CONVOLUTIONAL NEURAL NETWORK

The weights in the neural network can take both negative and positive values, whereas conductance values are strictly positive. To tackle this, we incorporate a parallel

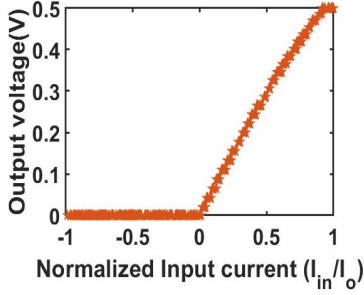


FIG. 8. Normalized output voltage versus normalized input current of the Max Pooled ReLU circuit with $I_0 = 10.67 \mu\text{A}$.

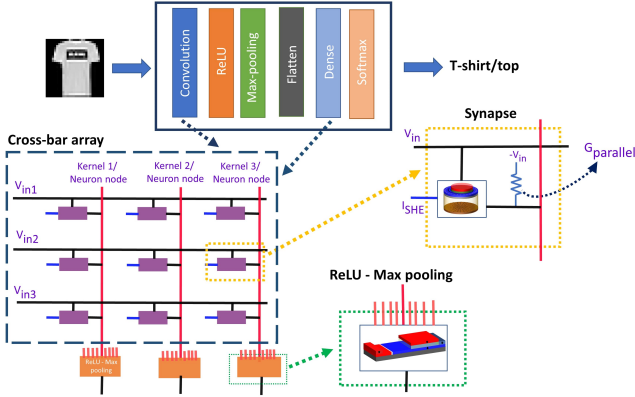


FIG. 9. CNN architecture for classifying fashion-MNIST and MNIST handwritten digits datasets. The convolution and dense layers are implemented using the cross-bar structure, where the input is applied to the horizontal lines while the vertical lines represents the kernel in convolution operation and neuron nodes in fully-connected dense layer. The skyrmion device along with the parallel conductance is used to store the weight in the cross-bar array. This convolution crossbar array is then connected to the domain-wall based ReLU-max pooling circuit to complete the feature extraction stage of the CNN.

conductance ($G_{parallel}$) with a negative input, allowing the synapses to effectively represent weights as shown in Fig. 9.

$$W_{i,j} = G_{skymion(i,j)} - G_{parallel} \quad (17)$$

$$G_{parallel} = \frac{G_{min} + G_{max}}{2} \quad (18)$$

where, $W_{i,j}$ is the weight connecting i^{th} row/input with j^{th} kernel/node, $G_{skymion}$ is the conductance of the skyrmion device and $G_{parallel}$ is the conductance of the device parallel to the skyrmion device. G_{min} and G_{max} are the minimum and maximum conductance values of the skyrmion device. The CNN training process is designed to ensure that the weights remain within the ± 1 range.

Convolutional Neural Networks (CNNs) are highly

TABLE V. CNN accuracy's

| Dataset | MNIST Hand-written dataset (%) | fashion-MNIST dataset (%) |
|-------------------|--------------------------------|---------------------------|
| Software Training | 99.85 | 94.52 |
| Software Testing | 98.35 | 90.63 |
| 4-bit Inference | 98.07 | 90.33 |
| 5-bit Inference | 98.01 | 90.52 |
| 6-bit Inference | 97.97 | 90.59 |

valuable in various machine learning tasks related to images, such as computer vision and image recognition [64]. The CNN architecture used for classifying MNIST handwritten digits and fashion-MNIST datasets is illustrated in Figure 9. The accuracy for MNIST handwritten digits and fashion-MNIST datasets is depicted in Figures 10(a) and 10(b), respectively. The accuracies after the 25th epoch are presented in Table V, demonstrating that the inference accuracies closely align with the software testing accuracy. This indicates the effectiveness of our skyrmion synapse and CMOS hybrid domain wall ReLU-max pooling devices. Our results indicate that good inference results can be achieved even with a 4-bit synapse.

VI. CONCLUSION

In conclusion, the paper presents multiple skyrmionic synapse device(4-bit,5-bit, and 6-bit) designed with skyrmions as neurotransmitters driven by the current-induced torque under two kinds of uniaxial anisotropy profiles enabling a constricted and aligned motion of the skyrmions nucleated circularly along the circumference of the FM disk facilitating the change in weights. The skyrmionic synapse device changes the conductance according to the number of skyrmions under the detector region or the post-synapse region. The highly desired synaptic property of symmetric and linear weight

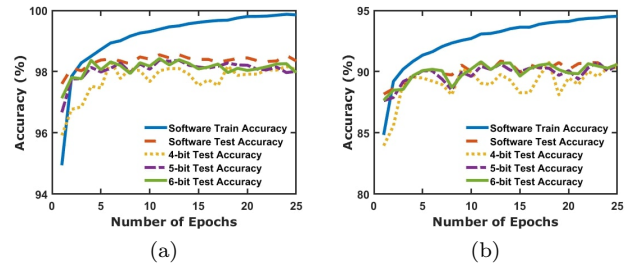


FIG. 10. Classification accuracy of the CNN for software training and testing along with the inference accuracy using 4-bit, 5-bit, and 6-bit synapses(concentric Ku profiles) for both (a) MNIST handwritten digits dataset and (b) Fashion-MNIST dataset.

update during the LTP and LTD operation is achieved without any additional techniques. Mitigating nonlinear weight update[65, 66] characteristic is a major challenge in the synaptic devices from which our proposed device is immune. Additionally, we have designed a 9-Input ReLU-Max pooled circuit using a hybrid CMOS-SOT-driven domain wall device that can be directly integrated with the crossbar array. The continuous variation of the domain wall position with current corresponds to a linear change in resistance, under the influence of uniaxial anisotropy variation enacting ReLU functionality. We evaluated the Convolutional Neural Network(CNN) using our proposed skyrmionic synaptic devices(as crossbar elements to implement the convolutional layer), Hybrid CMOS-SOT-driven domain wall-based ReLU max pooled circuit(as the activation and pooling layer)proving a com-

prehensive model for a full hardware CNN application. The CNN was trained using deep learning techniques to perform pattern recognition tasks with an accuracy of 98.07% employing the MNIST hand-written digit data set. Our work extends the scope for designing a full-hardware-based neuromorphic computing platform employing spintronic devices by coupling an atomistic description to circuit modeling.

ACKNOWLEDGEMENTS

The author BM wishes to acknowledge the support by the Science and Engineering Research Board (SERB), Government of India, Grant No. MTR/2021/000388.

-
- [1] E. Nature, Big data needs a hardware revolution, *Nature* **554**, 145 (2018).
- [2] S. Furber, Large-scale neuromorphic computing systems, *Journal of neural engineering* **13**, 051001 (2016).
- [3] J. Grollier, D. Querlioz, K. Camsari, K. Everschor-Sitte, S. Fukami, and M. Stiles, Neuromorphic spintronics. *nat. electron.* **3**, 360–370 (2020).
- [4] S. Liu, G. Wang, T. Bai, K. Mo, J. Chen, W. Mao, W. Wang, Z. Yuan, and B. Pan, Magnetic skyrmion-based spiking neural network for pattern recognition, *Applied Sciences* **12**, 9698 (2022).
- [5] D. Wang, R. Tang, H. Lin, L. Liu, N. Xu, Y. Sun, X. Zhao, Z. Wang, D. Wang, Z. Mai, *et al.*, Spintronic leaky-integrate-fire spiking neurons with self-reset and winner-takes-all for neuromorphic computing, *Nature Communications* **14**, 1068 (2023).
- [6] K. M. Song, J.-S. Jeong, B. Pan, X. Zhang, J. Xia, S. Cha, T.-E. Park, K. Kim, S. Finizio, J. Raabe, *et al.*, Skyrmion-based artificial synapses for neuromorphic computing, *Nature Electronics* **3**, 148 (2020).
- [7] P. Jadaun, C. Cui, S. Liu, and J. A. C. Inorvia, Adaptive cognition implemented with a context-aware and flexible neuron for next-generation artificial intelligence, *PNAS nexus* **1**, pgac206 (2022).
- [8] T. P. Xiao, C. H. Bennett, X. Hu, B. Feinberg, R. Jacobs-Gedrim, S. Agarwal, J. S. Brunhaver, J. S. Friedman, J. A. C. Inorvia, and M. J. Marinella, Energy and performance benchmarking of a domain wall-magnetic tunnel junction multibit adder, *IEEE Journal on Exploratory Solid-State Computational Devices and Circuits* **5**, 188 (2019).
- [9] A. Fert, N. Reyren, and V. Cros, Magnetic skyrmions: advances in physics and potential applications, *Nature Reviews Materials* **2**, 1 (2017).
- [10] N. Sisodia, J. Pelloux-Prayer, L. D. Buda-Prejbeanu, L. Anghel, G. Gaudin, and O. Boulle, Robust and programmable logic-in-memory devices exploiting skyrmion confinement and channeling using local energy barriers, *Physical Review Applied* **18**, 014025 (2022).
- [11] A. Fert, V. Cros, and J. Sampaio, Skyrmions on the track, *Nature nanotechnology* **8**, 152 (2013).
- [12] N. Nagaosa and Y. Tokura, Topological properties and dynamics of magnetic skyrmions, *Nature nanotechnology* **8**, 899 (2013).
- [13] D. Bhowmik, U. Saxena, A. Dankar, A. Verma, D. Kaushik, S. Chatterjee, and U. Singh, On-chip learning for domain wall synapse based fully connected neural network, *Journal of Magnetism and Magnetic Materials* **489**, 165434 (2019).
- [14] D. Kumar, H. J. Chung, J. Chan, T. Jin, S. T. Lim, S. S. Parkin, R. Sbiaa, and S. Piramanayagam, Ultralow energy domain wall device for spin-based neuromorphic computing, *ACS nano* **17**, 6261 (2023).
- [15] R. S. Yadav, P. Gupta, A. Holla, K. I. Ali Khan, P. K. Muduli, and D. Bhowmik, Demonstration of synaptic behavior in a heavy-metal-ferromagnetic-metal-oxide-heterostructure-based spintronic device for on-chip learning in crossbar-array-based neural networks, *ACS Applied Electronic Materials* **5**, 484 (2023).
- [16] R. S. Yadav, A. Sadashiva, A. Holla, P. K. Muduli, and D. Bhowmik, Impact of edge defects on the synaptic characteristic of a ferromagnetic domain-wall device and on on-chip learning, *Neuromorphic Computing and Engineering* **3**, 034006 (2023).
- [17] P. Metaxas, J. Jamet, A. Mougou, M. Cormier, J. Ferré, V. Baltz, B. Rodmacq, B. Dieny, and R. Stamps, Creep and flow regimes of magnetic domain-wall motion in ultrathin pt/co/pt films;? format?i with perpendicular anisotropy, *Physical review letters* **99**, 217208 (2007).
- [18] P. J. Metaxas, Creep and flow dynamics of magnetic domain walls: weak disorder, wall binding, and periodic pinning, in *Solid State Physics*, Vol. 62 (Elsevier, 2010) pp. 75–162.
- [19] D. K. Ojha, Y.-H. Huang, Y.-L. Lin, R. Chatterjee, W.-Y. Chang, and Y.-C. Tseng, Neuromorphic computing with emerging antiferromagnetic ordering in spin-orbit torque devices, *Nano Letters* (2024).
- [20] X. Han, Z. Wang, Y. Wang, D. Wang, L. Zheng, L. Zhao, Q. Huang, Q. Cao, Y. Chen, L. Bai, *et al.*, Neuromorphic computing in synthetic antiferromagnets by spin-orbit torque induced magnetic-field-free magnetization switching, *Advanced Functional Materials* , 2404679 (2024).

- [21] V. B. Desai, D. Kaushik, J. Sharda, and D. Bhowmik, On-chip learning of a domain-wall-synapse-crossbar-array-based convolutional neural network, *Neuromorphic Computing and Engineering* **2**, 024006 (2022).
- [22] Z. He and D. Fan, A tunable magnetic skyrmion neuron cluster for energy efficient artificial neural network, in *Design, Automation & Test in Europe Conference & Exhibition (DATE), 2017* (IEEE, 2017) pp. 350–355.
- [23] D. Das, Y. Cen, J. Wang, and X. Fong, Bilayer-skyrmion-based design of neuron and synapse for spiking neural network, *Physical Review Applied* **19**, 024063 (2023).
- [24] U. Saxena, D. Kaushik, M. Bansal, U. Sahu, and D. Bhowmik, Low-energy implementation of feed-forward neural network with back-propagation algorithm using a spin-orbit torque driven skyrmionic device, *IEEE Transactions on Magnetics* **54**, 1 (2018).
- [25] V. Vadde, B. Muralidharan, and A. Sharma, Power efficient relu design for neuromorphic computing using spin hall effect, *Journal of Physics D: Applied Physics* (2023).
- [26] C. Phatak, A. Petford-Long, and O. Heinonen, Direct observation of unconventional topological spin structure in coupled magnetic discs, *Physical review letters* **108**, 067205 (2012).
- [27] S. Wintz, C. Bunce, A. Neudert, M. Körner, T. Strache, M. Buhl, A. Erbe, S. Gemming, J. Raabe, C. Quitmann, *et al.*, Topology and origin of effective spin meron pairs in ferromagnetic multilayer elements, *Physical review letters* **110**, 177201 (2013).
- [28] S. Li, A. Du, Y. Wang, X. Wang, X. Zhang, H. Cheng, W. Cai, S. Lu, K. Cao, B. Pan, *et al.*, Experimental demonstration of skyrmionic magnetic tunnel junction at room temperature, *Science Bulletin* **67**, 691 (2022).
- [29] Y. Huang, W. Kang, X. Zhang, Y. Zhou, and W. Zhao, Magnetic skyrmion-based synaptic devices, *Nanotechnology* **28**, 08LT02 (2017).
- [30] C. Balan, J. W. van der Jagt, A. Fassatoui, J. Peña Garcia, V. Jeudy, A. Thiaville, M. Bonfim, J. Vogel, L. Ranno, D. Ravelosona, *et al.*, Improving néel domain walls dynamics and skyrmion stability using he ion irradiation, *Small* **19**, 2302039 (2023).
- [31] R. Juge, K. Bairagi, K. G. Rana, J. Vogel, M. Sall, D. Maily, V. T. Pham, Q. Zhang, N. Sisodia, M. Forster, *et al.*, Helium ions put magnetic skyrmions on the track, *Nano Letters* **21**, 2989 (2021).
- [32] H. Xia, C. Song, C. Jin, J. Wang, J. Wang, and Q. Liu, Skyrmion motion driven by the gradient of voltage-controlled magnetic anisotropy, *Journal of Magnetism and Magnetic Materials* **458**, 57 (2018).
- [33] A. Fassatoui, L. Ranno, J. PenaGarcia, C. Balan, J. Vogel, H. Béa, and S. Pizzini, Kinetics of ion migration in the electric field-driven manipulation of magnetic anisotropy of pt/co/oxide multilayers, *Small* **17**, 2102427 (2021).
- [34] S. Emori, E. Martinez, K.-J. Lee, H.-W. Lee, U. Bauer, S.-M. Ahn, P. Agrawal, D. C. Bono, and G. S. Beach, Spin hall torque magnetometry of dzyaloshinskii domain walls, *Physical Review B* **90**, 184427 (2014).
- [35] K.-S. Ryu, L. Thomas, S.-H. Yang, and S. S. Parkin, Current induced tilting of domain walls in high velocity motion along perpendicularly magnetized micron-sized co/ni/co racetracks, *Applied Physics Express* **5**, 093006 (2012).
- [36] D. Kumar, T. Jin, R. Sbiaa, M. Kläui, S. Bedanta, S. Fukami, D. Ravelosona, S.-H. Yang, X. Liu, and S. P. ramanayagam, Domain wall memory: Physics, materials, and devices, *Physics Reports* **958**, 1 (2022).
- [37] L. Zhu, D. C. Ralph, and R. A. Buhrman, Highly efficient spin-current generation by the spin hall effect in au 1- x pt x, *Physical Review Applied* **10**, 031001 (2018).
- [38] E. Raymenants, O. Bultynck, D. Wan, T. Devolder, K. Garello, L. Souriau, A. Thiam, D. Tsvetanova, Y. Canvel, D. Nikonov, *et al.*, Nanoscale domain wall devices with magnetic tunnel junction read and write, *Nature Electronics* **4**, 392 (2021).
- [39] D. Kaushik, U. Singh, U. Sahu, I. Sreedevi, and D. Bhowmik, Comparing domain wall synapse with other non volatile memory devices for on-chip learning in analog hardware neural network, *AIP Advances* **10** (2020).
- [40] E. Liu, Y.-C. Wu, S. Couet, S. Mertens, S. Rao, W. Kim, K. Garello, D. Crotti, S. Van Elshocht, J. De Boeck, *et al.*, Synthetic-ferromagnet pinning layers enabling top-pinned magnetic tunnel junctions for high-density embedded magnetic random-access memory, *Physical Review Applied* **10**, 054054 (2018).
- [41] Y. Zhang, S. Luo, X. Yang, and C. Yang, Spin-orbit-torque-induced magnetic domain wall motion in ta/cofe nanowires with sloped perpendicular magnetic anisotropy, *Scientific reports* **7**, 2047 (2017).
- [42] J. Chureemart, S. Boonchui, R. Chantrell, P. Chureemart, *et al.*, Current-induced domain wall motion: Comparison of stt and she, *Journal of Magnetism and Magnetic Materials* **529**, 167838 (2021).
- [43] C. O. Avci, E. Rosenberg, M. Baumgartner, L. Beran, A. Quindeau, P. Gambardella, C. A. Ross, and G. S. Beach, Fast switching and signature of efficient domain wall motion driven by spin-orbit torques in a perpendicular anisotropy magnetic insulator/pt bilayer, *Applied Physics Letters* **111** (2017).
- [44] V. Vadde, B. Muralidharan, and A. Sharma, Orthogonal spin current injected magnetic tunnel junction for convolutional neural networks, *IEEE Transactions on Electron Devices* (2023).
- [45] M. J. Donahue and D. G. Porter, Oommf user’s guide, version 1.0 (1999).
- [46] J. Sampaio, V. Cros, S. Rohart, A. Thiaville, and A. Fert, Nucleation, stability and current-induced motion of isolated magnetic skyrmions in nanostructures, *Nature nanotechnology* **8**, 839 (2013).
- [47] S. Yang, J. W. Son, T.-S. Ju, D. M. Tran, H.-S. Han, S. Park, B. H. Park, K.-W. Moon, and C. Hwang, Magnetic skyrmion transistor gated with voltage-controlled magnetic anisotropy, *Advanced Materials* **35**, 2208881 (2023).
- [48] J. J. Joos, P. Bassirian, P. Gypens, J. Mulkers, K. Litzius, B. Van Waeyenberge, and J. Leliaert, Tutorial: Simulating modern magnetic material systems in mumax3, *Journal of Applied Physics* **134** (2023).
- [49] J. Hirsch, Spin hall effect, *Physical review letters* **83**, 1834 (1999).
- [50] S. Takahashi and S. Maekawa, Spin current, spin accumulation and spin hall effect, *Science and Technology of Advanced Materials* **9**, 014105 (2008).
- [51] K. Sawada, T. Uemura, M. Masuda, K.-i. Matsuda, and M. Yamamoto, Tunneling magnetoresistance simulation used to detect domain-wall structures and their motion in a ferromagnetic wire, *IEEE transactions on magnetics* **45**, 3780 (2009).

- [52] M. Tanaka and Y. Higo, Large tunneling magnetoresistance in gammas/aldas/gammas ferromagnetic semiconductor tunnel junctions, *Physical Review Letters* **87**, 026602 (2001).
- [53] M. Julliere, Tunneling between ferromagnetic films, *Physics letters A* **54**, 225 (1975).
- [54] J. C. Slonczewski, Conductance and exchange coupling of two ferromagnets separated by a tunneling barrier, *Physical Review B* **39**, 6995 (1989).
- [55] A. Fert, J.-L. Duvail, and T. Valet, Spin relaxation effects in the perpendicular magnetoresistance of magnetic multilayers, *Physical Review B* **52**, 6513 (1995).
- [56] T. Valet and A. Fert, Theory of the perpendicular magnetoresistance in magnetic multilayers, *Physical Review B* **48**, 7099 (1993).
- [57] T. G. Rijk, R. Coehoorn, and W. De Jonge, Combined spin valve and anisotropic magnetoresistance in nife/cu/nife layered thin films, *MRS Online Proceedings Library (OPL)* **313** (1993).
- [58] E. Milosevic, S. Kerdsonpanya, and D. Gall, The resistivity size effect in epitaxial ru (0001) and co (0001) layers, in *2018 IEEE Nanotechnology Symposium (ANTS)* (IEEE, 2018) pp. 1–5.
- [59] M.-H. Nguyen, D. Ralph, and R. Buhrman, Spin torque study of the spin hall conductivity and spin diffusion length in platinum thin films with varying resistivity, *Physical review letters* **116**, 126601 (2016).
- [60] L. G. Wen, C. Adelman, O. V. Pedreira, S. Dutta, M. Popovici, B. Briggs, N. Heylen, K. Vanstreels, C. J. Wilson, S. Van Elshocht, *et al.*, Ruthenium metallization for advanced interconnects, in *2016 IEEE International Interconnect Technology Conference/Advanced Metallization Conference (iitc/amc)* (IEEE, 2016) pp. 34–36.
- [61] H. Y. T. Nguyen, W. Pratt Jr, and J. Bass, Spin-flipping in pt and at co/pt interfaces, *Journal of magnetism and magnetic materials* **361**, 30 (2014).
- [62] M. A. Khasawneh, C. Klose, W. Pratt Jr, and N. O. Birge, Spin-memory loss at co/ru interfaces, *Physical Review B* **84**, 014425 (2011).
- [63] A. Sharma, J. Romero, N. Theodoropoulou, R. Loloee, W. Pratt, and J. Bass, Specific resistance and scattering asymmetry of py/pd, fe/v, fe/nb, and co/pt interfaces, *Journal of Applied Physics* **102** (2007).
- [64] I. Goodfellow, Y. Bengio, and A. Courville, *Deep learning* (MIT press, 2016).
- [65] I. Boybat, M. Le Gallo, S. Nandakumar, T. Moraitis, T. Parnell, T. Tuma, B. Rajendran, Y. Leblebici, A. Sebastian, and E. Eleftheriou, Neuromorphic computing with multi-memristive synapses, *Nature communications* **9**, 2514 (2018).
- [66] J. Lee, J. Hwang, Y. Cho, M.-K. Park, W. Y. Choi, S. Kim, and J.-H. Lee, Crus: A hardware-efficient algorithm mitigating highly nonlinear weight update in cim crossbar arrays for artificial neural networks, *IEEE Journal on Exploratory Solid-State Computational Devices and Circuits* **8**, 145 (2022).
- [67] T. Yokouchi, S. Sugimoto, B. Rana, S. Seki, N. Ogawa, Y. Shiomi, S. Kasai, and Y. Otani, Pattern recognition with neuromorphic computing using magnetic field-induced dynamics of skyrmions, *Science Advances* **8**, eabq5652 (2022).
- [68] H. Liu and T. Ohsawa, A binarized spiking neural network based on auto-reset lif neurons and large signal synapses using stt-mtjs, *Japanese journal of applied physics* **62**, 044501 (2023).
- [69] S. Soni, G. Verma, H. Nehete, and B. K. Kaushik, Energy efficient spin-based implementation of neuromorphic functions in cnns, *IEEE Open Journal of Nanotechnology* **4**, 102 (2023).
- [70] A. Sengupta, Y. Shim, and K. Roy, Proposal for an all-spin artificial neural network: Emulating neural and synaptic functionalities through domain wall motion in ferromagnets, *IEEE Transactions on Biomedical Circuits and Systems* **10**, 1152 (2016).
- [71] M. Sharad, C. Augustine, G. Panagopoulos, and K. Roy, Spin based neuron-synapse module for ultra low power programmable computational networks, in *The 2012 International Joint Conference on Neural Networks (IJCNN)* (2012) pp. 1–7.
- [72] D. Zhang, L. Zeng, K. Cao, M. Wang, S. Peng, Y. Zhang, Y. Zhang, J.-O. Klein, Y. Wang, and W. Zhao, All spin artificial neural networks based on compound spintronic synapse and neuron, *IEEE Transactions on Biomedical Circuits and Systems* **10**, 828 (2016).
- [73] X. Hu, C. Cui, S. Liu, F. Garcia-Sanchez, W. H. Brigner, B. W. Walker, A. J. Edwards, T. P. Xiao, C. H. Bennett, N. Hassan, *et al.*, Magnetic skyrmions and domain walls for logical and neuromorphic computing, *Neuromorphic Computing and Engineering* **3**, 022003 (2023).